Remote Sensing of Environment 115 (2011) 2861–2873

Contents lists available at ScienceDirect

Remote Sensing of Environment

journal homepage: www.elsevier.com/locate/rse

# Measuring biomass changes due to woody encroachment and deforestation/degradation in a forest–savanna boundary region of central Africa using multi-temporal L-band radar backscatter

E.T.A. Mitchard [a,*], S.S. Saatchi [b], S.L. Lewis [c], T.R. Feldpausch [c], I.H. Woodhouse [a], B. Sonké [d], C. Rowland [e], P. Meir [a]

[a] School of GeoSciences, University of Edinburgh, EH8 9XP, UK
[b] Jet Propulsion Laboratory, California Institute of Technology, Pasadena, CA 91109, USA
[c] Earth and Biosphere Institute, School of Geography, University of Leeds, LS2 9JT, UK
[d] Department of Biology, University of Yaoundé 1, P.O. Box 047, Yaoundé, Cameroon
[e] CEH Lancaster, Lancaster Environment Centre, Lancaster, LA1 4AP, UK

ARTICLE INFO

*Article history:*
Received 9 April 2009
Received in revised form 12 October 2009
Accepted 7 February 2010
Available online 6 May 2011

*Keywords:*
ALOS PALSAR
Aboveground biomass
Cameroon
Change detection
Deforestation
Degradation
Ecotone
Forest–savanna boundary
JERS-1
SAR
Radar
REDD
Woody encroachment

ABSTRACT

Satellite L-band synthetic aperture radar backscatter data from 1996 and 2007 (from JERS-1 and ALOS PALSAR respectively), were used with field data collected in 2007 and a back-calibration method to produce biomass maps of a 15 000 km$^2$ forest–savanna ecotone region of central Cameroon. The relationship between the radar backscatter and aboveground biomass (AGB) was strong ($r^2 = 0.86$ for ALOS HV to biomass plots, $r^2 = 0.95$ relating ALOS-derived biomass for 40 suspected unchanged regions to JERS-1 HH). The root mean square error (RMSE) associated with AGB estimation varied from ~25% for AGB < 100 Mg ha$^{-1}$ to ~40% for AGB > 100 Mg ha$^{-1}$ for the ALOS HV data. Change detection showed a significant loss of AGB over high biomass forests, due to suspected deforestation and degradation, and significant biomass gains along the forest–savanna boundary, particularly in areas of low population density. Analysis of the errors involved showed that radar data can detect changes in broad AGB class in forest–savanna transition areas with an accuracy >95%. However, quantitative assessment of changes in AGB in Mg ha$^{-1}$ at a pixel level will require radar images from sensors with similar characteristics collecting data from the same season over multiple years.



## 1. Introduction

The interface between tropical forest and savanna in west and central Africa is a wide, structurally and floristically diverse mosaic of vegetation types, with forest penetrating deeply into the savanna biome as gallery forests along river banks, and also as forest patches on plateaus and in between rivers (Dai et al., 2004; Hely et al., 2006; Menaut, 1983). The savannas in this region are not maintained by precipitation, there being enough rainfall to support full canopy closure except in the poorest or inundated soils. Instead they are maintained largely by anthropogenic disturbance such as fire and clearance for grazing, agriculture and timber (Bucini & Hanan, 2007; Sankaran et al., 2005). Changes in these disturbance regimes can therefore result in rapid changes in the woody cover of this region. Due to the large extent of the tropical forest–savanna ecotone in Africa (1.28 million km$^2$ is forest–savanna mosaic, compared with 2.36 million km$^2$ forest and 4.12 million km$^2$ woodland; Mayaux et al., 2004), any changes in the woody vegetation cover and the resulting feedbacks could have significant implications for biodiversity and the carbon cycle (Lewis, 2006). Such ecotones are also important as they are transitional habitats that appear to be areas of evolutionary dynamism, storing genetic diversity and acting as an important locus for the generation of new species (Smith et al., 1997, 2001).

Dynamics of woody vegetation in this ecotone are the result of the integration of a variety of different competing processes, each of largely unknown magnitude and spatial distribution. Forest is being cleared for agriculture, and woody savannas are often burnt to assist agriculture and cattle grazing (FAO, 2007; Zhang et al., 2006). Forest and woody savannas are also undergoing degradation, especially around settlements, for timber (legal logging concessions and illegal

* Corresponding author.
*E-mail address:* edward.mitchard@ed.ac.uk (E.T.A. Mitchard).

0034-4257/$ – see front matter 
doi:10.1016/j.rse.2010.02.022

extraction), wood fuel and charcoal (Goetze et al., 2006; Mertens & Lambin, 2000). Changes in climate also have the potential to alter the area of forest and savanna, for example increases in dry season length will favor savanna, as would rising temperatures (Dai et al., 2004; Hely et al., 2006; Zeng & Neelin, 2000). In contrast, there are also processes that could cause forest to expand into savanna and savannas to increase in woodiness: reduced anthropogenic fire, caused by reduced human activity in an area; increased $CO_2$ concentration, which has the potential to increase tree growth in forests and therefore biomass (Lewis et al., 2004, 2009) by favoring the growth of trees with a C3 photosynthetic pathway, over grasses that have a C4 pathway[1] (Lloyd & Farquhar, 1996, 2008); and if rainfall increased, which would again favor trees over grasses (Hely et al., 2006).

It has been suggested that forest is expanding into savannas in central Africa because of urban-migration and a consequent reduction in fire frequency (Boulvert, 1990). Indeed, this forest encroachment has been found to be occurring in other tropical forest–savanna ecotones, including northern Australia (Bowman et al., 2001; Brook & Bowman, 2006; Hopkins et al., 1996), the Western Ghats of India (Puyravaud et al., 2003), and South America (Duarte et al., 2006; Durigan & Ratter, 2006; Marimon et al., 2006). However, little quantitative analysis followed Boulvert's initial observations in Africa: a literature search found only three studies reporting woody expansion in African tropical forest–savanna transitions, though there is much evidence of woody encroachment in semi-arid environments in Africa (Archer et al., 2001; Eamus & Palmer, 2007). In an ecotonal region of central Cameroon, optical remote sensing data and field measurements were used to show that over a period of 40 years (1950–1990), gallery forests encroached into the savanna landscape at a rate of 0.6 to 2 m a year (Happi, 1998). In eastern Cameroon, analysis of soil carbon isotopes ($^{13}C/^{12}C$, $^{14}C$) along two transects showed both significant expansion of the forest, and that increased woody cover of the savanna has occurred over the past century (Guillet et al., 2001). In Budongo Forest Reserve, Uganda, a combination of field studies and vegetation index-based satellite change detection were used to demonstrate a 14% increase in woody vegetation (Nangendo, 2005). In combination, these studies provide some evidence that forest expansion is occurring, but none used a method that can be extrapolated to larger areas without a huge investment of resources: all involved extensive field studies or the manual interpretation of high-resolution remotely sensed images.

The use of space-borne radar backscatter data is becoming increasingly accepted as a useful method for measuring woody biomass over much larger areas in the tropics because of the capability of radar to penetrate through the forest canopy, and its capacity for all-weather acquisition (Lu, 2006; Ribeiro et al., 2008; Sano et al., 2005; Santos et al., 2002). Radar data are likely to be particularly applicable to forest–savanna boundary regions, as theory suggests there will be a substantial increase in backscatter as both the density and size of trees increase (Podest & Saatchi, 2002; Woodhouse, 2006), and biomass changes from savanna to forest are in the lower biomass ranges, where radar is most sensitive. As radar backscatter responds to the density, size, orientation, and water content of scattering elements on the surface (Rosenqvist et al., 2007), rather than just the color and density of leaves, it has the potential to be more sensitive to changes in the woodiness of savanna than spectral data. This is especially true because the radar signal will be much less sensitive to grasses than spectral data, especially when longer radar wavelengths are used. The spectral vegetation signal from trees can be very hard to distinguish from that of grasses unless hyperspatial data, capable of resolving individual trees (Lu, 2006), or multi-temporal data which enables the phenology of different landcover types to be separated (Loveland et al., 2000), are used.

The successful launch of the Advanced Land Observing Sattelite's Phased Array-type L-band Synthetic Aperture Radar (ALOS PALSAR) in 2006 has increased the potential to use radar to measure biomass, as this is the first long-wavelength (L-band, 23-cm wavelength) synthetic aperture radar (SAR) satellite sensor to have the capability of collecting cross-polarized (HV, horizontal-send, vertical receive) data in addition to horizontal-send, horizontal-receive (HH) data. This is an advantage for detecting biomass because for HV only scattering elements that change the polarization of the incoming electromagnetic radiation will be detected, so complex three-dimensional structures such as trees will produce a strong response, but soil moisture, which does not change the polarization of the incoming radiation, will not be detected.

Radar has been used only rarely to quantify biomass in forest–savanna transition regions, though when used it has been with considerable success (Lucas et al., 2000; Ribeiro et al., 2008; Sano et al., 2005; Santos et al., 2002). It has to our knowledge never previously been used for long-term biomass change detection in forest–savanna transition regions, despite the availability and potential of the data. Here, we compare satellite L-band radar data from 1996 and 2007 over a large ecotonal region of central Cameroon, both to assess changes in aboveground woody biomass in this region, and as a proof of concept for its application for large scale monitoring of changes in biomass from space.

## 2. Study area

The study area covers a 15 000 $km^2$ region in central Cameroon, centered around 6°4′18″ N, 12°53′18″ E, encompassing the Mbam Djerem National Park and the surrounding area to the north and east (Fig. 1). This region was chosen as it extends across a range of tropical vegetation types, from humid forests contiguous with the Congo Basin tropical forest belt in the south to savanna with narrow gallery forests in the north. It experiences an annual rainfall of 1720 mm, with a standard deviation of 213 mm (derived from Tropical Rainfall Measuring Mission (TRMM) 3B43 V6 data from January 1998 to December 2008). There is a pronounced dry season from December to March, with an average rainfall of 20 mm per month. The Mbam Djerem National park was established in the year 2000 as an expanded version of the longer-standing Pangare Djerem reserve with funds from Chad-Cameroon Pipeline Project, and is currently maintained by the Wildlife Conservation Society. It has a high species diversity, containing over 360 bird and 50 mammal species (Anonymous, 2007), and is regarded as having critical importance for the preservation of Central African biodiversity (Doumenge et al., 2003). The park itself has a very low human population density, with almost no permanent residents. Major anthropogenic disturbances in the park are fishing, bushmeat hunting in the southern forests, and grazing accompanied by burning in areas along the northern forest–savanna boundary. The regions surrounding the park are more populated, especially on the eastern side, with the two major towns being Tibati on the western side of Lake Mbakaou, and Ngaoundal in the northeast of the study area. The population of both towns has increased by approximately 85% in the past twenty years, from 15 522 and 11 382 respectively in 1987 to 28 981 and 21 239 in 2006 (CIESIN, 2004; PNUD, 1999).

[1] C3 photosynthesis is the photosynthetic pathway that occurs in most plants including all trees. C4 photosynthesis is an alternative used by some grasses, including the majority found in this area, that gives increased efficiency of photosynthesis with respect to water 'use' (i.e. water loss through transpiration), and is therefore beneficial in drier and hotter environments (Taiz & Zeiger, 2006). However, the advantage which C4 plants have over C3 plants is reduced as the concentration of $CO_2$ in the atmosphere increases (energetically costly adaptations that increase the concentration of $CO_2$ in leaf cells becomes less advantageous; Lloyd & Farquhar, 2008). Thus increasing $CO_2$ concentrations could be responsible for woody encroachment by reducing the competitiveness of C4 grasses compared with C3 plants. However, increasing temperatures or a reduction in rainfall, that may occur concurrently with an increase in $CO_2$ concentration, could negate this effect by increasing the competitive advantage of C4 grasses over C3 trees.

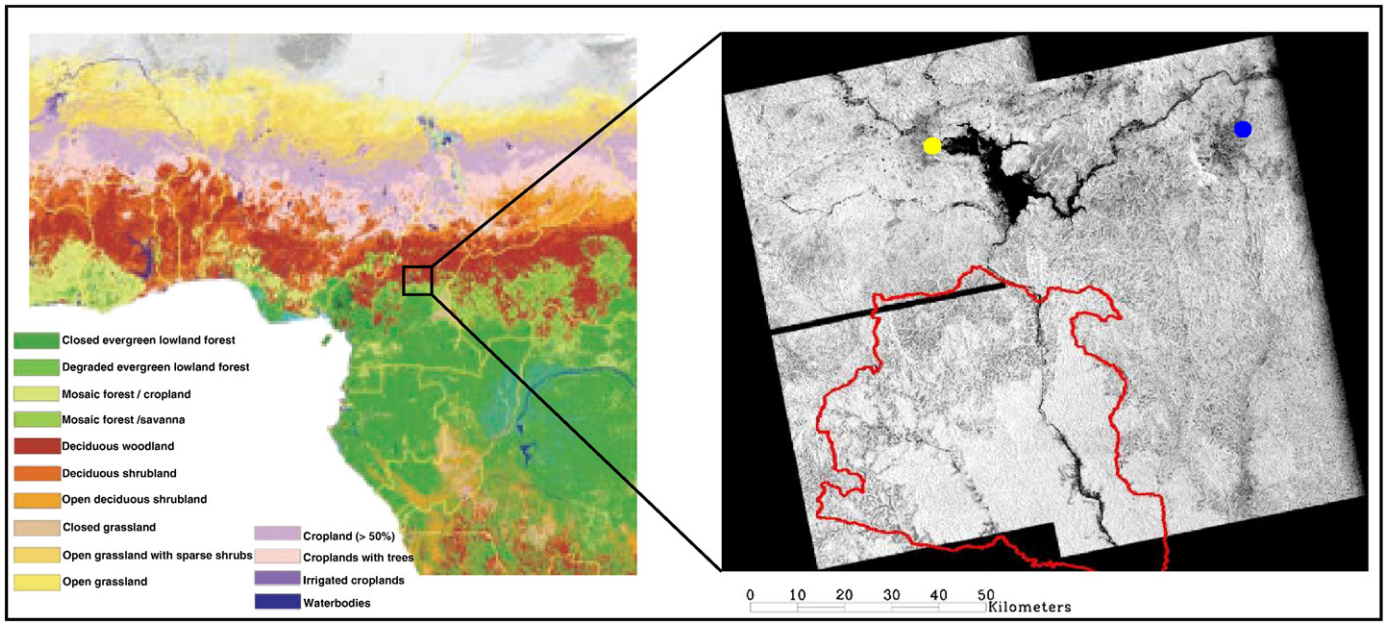


**Fig. 1.** A section of a vegetation map of Africa taken from Mayaux et al. (2004), showing the location of the study area within Cameroon, with the ALOS HV 2007 mosaic showing the Mbam Djerem National Park outlined in red, Tibati in yellow and Ngaoundal in blue.

## 3. Methods

### 3.1. Field data

The study area was visited in October–December 2007 as part of the Tropical Biomes in Transition project (TROBIT, www.geog.leeds.ac.uk/research/trobit). Vegetation was sampled in four regions from the top to the middle of the Mbam Djerem National Park. In all, data were collected from four one-hectare savanna plots, four one-hectare forest plots, a pair of 0.4 ha plots (one in transitional forest, one savanna), and eight $20\times200$ m transects ($8\times100$ m$\times100$ m; $2\times40$ m$\times100$ m; $8\times20$ m$\times200$ m). Seven transects ran from forest into savanna, and as the transition from forest to savanna was very sharp (typically occurring in under five meters), they were each split into a forest and a savanna portion, hence each giving two data points. We did not sub-divide these transects further (nor divide the ten larger plots), in order to remove any problems of autocorrelation: all data-points are sufficiently separated in space or vegetation type to be considered independent. One transect was solely located in forest, and for this AGB was averaged across its whole length. So, in total, 25 biomass plots were used in this study, 13 from forest and transitional forest, and 12 from savanna.

Within these 18 sampling locations data were collected for every tree with a diameter $\geq10$ cm at 1.3 m along the stem, or above buttresses or stem deformities, a forestry convention called 'diameter at breast height' (DBH). The variables used in this study were the species, DBH, and height (the latter measured for only a subset of trees). Height was estimated using vertex hypsometers (Laser Vertex Hypsometer/Vertex Hypsometer III, Haglöf, Sweden). The height of every tree was measured for the 8 transects and for the remaining 10 plots height was collected for only a random subsample of trees, and site-specific power-law regression equations used to estimate height from diameter for the remaining trees (average $n=56$ trees for each plot, average RMSE$<1.6$ m, $p<0.001$ in all cases). The field sites were located using a handheld differential GPS (Trimble GeoHX, Trimble, USA). The GPS positions were later corrected using data from the SOPAC N'Koltang ground station in Libreville, Gabon, using the H-STAR differential correction facility in the software GPS Pathfinder Office 3.10 (Trimble, USA), resulting in accuracies of $<0.5$ m in the horizontal direction and $<1$ m in the vertical.

The aboveground biomass (AGB) in kilograms of each tree was estimated using the optimal pan-tropical allometric equations as derived by Chave et al. (2005). For the savanna species the dry forest equation (Eq. 1) was used, for forest species the moist forest equation (Eq. 2) was used:

$$\mathrm{AGB} = exp\left[-2.187 + 0.916\ ln\left(\rho D^2 H\right)\right] \quad (1)$$

$$\mathrm{AGB} = exp\left[-2.977 + ln\left(\rho D^2 H\right)\right] \quad (2)$$

where $\rho$ is the wood mass density (oven-dry wood mass divided by green volume, g/cm$^3$), $D$ is the DBH in cm at 1.3 m, and $H$ is the tree height in meters. Species were differentiated into forest and savanna species based on knowledge of the ecology of the species from BS & SLL, and in which environment they were predominantly found. Wood mass density (also known as wood specific gravity) data were collated from the Global Wood Density Database (Chave et al., 2009; Zanne et al., 2009), in which wood density values measured at 12% or 18% moisture were converted to wood mass density. We also calculated biomass for the forest species using the dry forest allometric equation (Eq. 1). Though this reduced the biomass of the forest plots by 5–10%, this did not change any of the conclusions reported in the paper so the results are not shown.

The biomass values produced using the allometric equations and all three tree-specific variables were then summed and normalized by the area of the plots to produce estimates of woody AGB in Mg ha$^{-1}$. Stems with a DBH$<10$ cm were not measured for all plots, so the term AGB for the remainder of this paper refers to the dry biomass of stems with a DBH$\geq10$ cm, which are likely to comprise $>95\%$ of the woody biomass in these ecosystems (based on the 8 transects which were measured to a 5 cm minimum diameter, and pan-African estimates from Lewis et al., 2009). These larger trees will be the component to which L-band radar responds most strongly.

### 3.2. Remote sensing data

JERS-1 HH L-band SAR data were collated from the Global Rainforest Mapping Project (GRMP) (De Grandi et al., 2000), for the study area from the beginning and end of the dry season (November and March) of 1996. The scenes had been geometrically corrected, radiometrically calibrated, mosaicked into one image, and resampled from the original 12.5 m pixel spacing to 100 m pixels using wavelet decomposition, maintaining as much of the true signal as possible while greatly reducing speckle and noise (De Grandi et al., 2000). These data were converted from digital number (DN) to sigma$^0$ values using the equation and calibration coefficients provided by the GRMP (see http://southport.jpl.nasa.gov/GRFM/), using ENVI 4.4 (ITT, USA):

$$\text{sigma}^0[\text{dB}] = 20 \cdot \log_{10}(6 \cdot \text{DN} + 250) - 68.2. \quad (3)$$

The 2007 data comprised four ALOS PALSAR scenes collected in the FBD (Fine Beam Double-polarization) mode that were acquired from the Alaska Satellite Facility, having been provided to them by JAXA. Two were captured on the 26th July 2007, and the other two on the 12th of August 2007. These are, like the JERS data, L-band, but are polarimetric, including HH and HV polarizations, and were provided at the original 12.5 m pixel spacing.

Quickbird data (60 cm panchromatic resolution and 2.4 m multispectral resolution) were acquired from Eurimage for all the sites by purchasing an archive image from 19th February 2004 for the southern sites and requesting a new acquisition, captured on 30th January 2008, for the northern sites. These ground-point corrected Quickbird data are estimated to be geo-correct to <2 m. In order to reduce speckle noise, the ALOS image was resampled by averaging blocks of 2×2 pixels to produce an image at 25 m resolution. Areas of the ALOS scenes covering the field data plots were georeferenced by eye to the Quickbird data, by using 30 ground control points taken from features such as islands, small clumps of trees and branching points of gallery forests, with resulting RMSE<0.4 ALOS pixels (10 m).

The ALOS scenes were converted to sigma$^0$ values using the following equation and data-specific calibration factors, identical for all scenes:

$$\text{sigma}^0[\text{dB}] = 10\left(\log_{10}\text{DN}^2\right) + CF \quad (4)$$

where $CF$ is the calibration factor, set at −80.2 for the HV polarization and −83.2 for the HH polarization for scenes generated before 1st January 2009 (Shimada et al., 2009).

### 3.3. Radar sensitivity to structure and biomass

The sigma$^0$ values for pixels covering the plots were converted to the power domain before averaging, to ensure the use of the arithmetic, not geometric, means. Eighteen of the twenty-five biomass plots fell on the overlap between the two scenes captured seventeen days apart. A regression analysis between the two sets of backscatter values found that they were very well correlated ($dB_{SE} = 1.0074(dB_{SW})$, $r^2 = 0.88$, $p<0.00001$, where $dB_{SE}$ and $dB_{SW}$ are the sigma$^0$ HV backscatter values for the 18 sites found in both the south-east and south-west images respectively), and were not significantly different from each other (paired $t$-test of difference not equal to zero, $p = 0.384$), therefore the mean of the two raw power averages for each site was used in all presented analyses. The sigma$^0$ values for both polarizations were then regressed against structural features of the plots (basal area, average height, stem density and average DBH), and then against the AGB values for each site. Best fit empirical relationships were then calculated comparing backscatter with these variables, as no consensus has yet been reached as to what functional form *a priori* best describes these relationships. These comparisons with structural features are important as the majority of previous studies relating such data to backscatter are from temperate plantation forests (Lu, 2006; Woodhouse, 2005), and as such there is little data from natural heterogeneous tropical savanna–forest mosaics. All regression analyses were performed with the software SigmaPlot 10.0 (Systat Software, USA).

### 3.4. Biomass change detection

To allow comparison with the JERS data, the ALOS data were mosaicked and subsequently resampled to 100 m pixels. The JERS data were then georeferenced to the ALOS data using a network of 40 ground control points, selected by eye, which resulted in an RMSE of 0.48 pixels (48 m); areas in the JERS image not present in the ALOS mosaic were then masked.

As there were no field data available for this area from 1996, and the field data collected in 2007 is from areas near the forest edges that are suspected to have increased in biomass over the preceding eleven years (Mitchard et al., 2009), it was necessary to back-calibrate the JERS HH data to the ALOS-derived AGB values from areas that were unlikely to have changed over the time period. This methodology relies on the fact that there are identifiable areas where AGB is relatively stable in forest–savanna transition regions and the impacts of environmental variables on the radar backscatter such as soil and canopy moisture are relatively small (Hovestadt et al., 1999; Jeltsch et al., 1999; Ratter, 1992; Santos et al., 2002). Pixels were randomly selected from the image, and when they were judged to have fallen in an area that was unlikely to have changed (e.g. dense forest, or known grassland, confirmed by visual analysis of a Landsat ETM+ scene from 2000 compared with ASTER images from 2006/7), pixel values were extracted and averaged for a homogeneous area of 5×5 pixels around this pixel from both images (25 ha). These larger areas were used in order to limit errors caused by speckle and geolocation problems, with this averaging across homogeneous areas greatly increasing the confidence in the relationship produced. A regression between the ALOS-derived AGB values and the sigma$^0$ values from the JERS image was then performed, using the same relationship as with ALOS HH to ensure that the biomass of young and regenerating forests was calibrated correctly, and the derived relationship used to create a biomass map for the JERS image. Although there is evidence for a general increase in AGB across higher biomass tropical African forests (Lewis et al., 2009), at most this increase would be a small fraction of the total biomass of these sites (<4%), too small to be detectable by the radar backscatter data at these high biomass values. Hence we assumed that no detectable change had occurred in the AGB of the selected high biomass sites.

The accuracy of the derived relationship between JERS HH and AGB was evaluated by examining the relationship between ALOS HH and AGB, as both sensors have similar characteristics and incidence angles. We did not use the HH channel from both sensors to perform the change detection directly (using differences in dB value after a cross-calibration procedure) because the ALOS HH data were acquired in the wet season and as such were not comparable, as the HH channel responds strongly to soil moisture as well as to AGB.

The biomass class widths were chosen to be approximately equal to the RMSE of the biomass estimation at that level, and thus the classes increase in width as biomass increases, with the highest class taking as its lowest value the point where there is no evidence of a significant positive relationship between biomass and backscatter above that point. The area covered by the different classes at the two time points was compared, and a change map was produced showing the changes in average biomass at a 500 m (25 ha) resolution. Subsequently, an assessment of the sources and likely magnitude of uncertainties was performed.

## 4. Results

### 4.1. Field data

In total 4368 trees were measured, representing 205 species from 142 genera and 58 families. AGB measurements for the 25 data points ranged from 6 to 424 Mg ha$^{-1}$. Table 1 gives the full plot data combined with the ALOS HH and HV backscatter data. As expected biomass values were strongly related to basal area, with a fitted linear relationship giving an $r^2$ of 0.92 (Fig. 2). However the influence of height and wood density values on the biomass estimates using these equations can be seen here, as if an allometric equation that used only DBH values had been used this relationship would have an $r^2$ of 1. Biomass was also significantly related to average height ($r^2=0.70$) and to stem density ($r^2=0.45$), though in both cases the quadratic terms were significant in the regression, suggesting a reduction in the strength of the relationship at higher biomass values. There was a weaker but still significant correlation between biomass and the average DBH for each plot when a quadratic relationship was fitted ($r^2=0.30$, $p<0.01$).

### 4.2. ALOS backscatter sensitivity to vegetation structure

Significant log relationships were found between ALOS HV and HH sigma$^0$ backscatter and basal area, average height, and stem density (Fig. 3). No significant relationship was found between average DBH for the plot and either polarization. As expected, both polarizations responded most strongly to basal area (HV: $r^2=0.76$, HH: $r^2=0.55$), with HV having the smaller residuals. HV backscatter responded almost as strongly to average height ($r^2=0.73$), though HH responded less strongly to this variable ($r^2=0.48$). A loss of sensitivity appeared to occur quite early in both cases, with a strong relationship with height up to about 9 m and little evidence of a predictive relationship above this point. There was a significant response to stem density in both polarizations (HV $r^2=0.47$, $p<0.0005$, HH $r^2=0.48$, $p<0.0001$); interestingly in this case, HH is more strongly correlated than HV, even if only marginally and insignificantly so. This is possibly due to the influence of ground-trunk scattering, which should increase with stem density, and is a more influential component of the HH than HV backscatter (Woodhouse, 2005).

### 4.3. ALOS to biomass regression

One biomass plot was on a significant slope (*c.* 25°), in radar shadow, and consequently had an anomalously low radar return (Woodhouse, 2005). It was therefore thought most appropriate to remove this point from subsequent analyses, as all other plots were located on comparatively flat ground (0°–7° slope), and therefore were unsuitable for developing and testing a slope-correction procedure to apply to the anomalous plot. Attempts were made to fit a relationship between AGB and a combination of HH and HV polarizations, however the strongest relationship was found between ALOS HV sigma$^0$ alone and AGB, using an exponential rise-to-maximum model, as this best fitted the backscatter data, with the loss of sensitivity at approximately 150–200 Mg ha$^{-1}$ well modeled (see Fig. 4a). This fitted model happens to be equivalent to the simple Water Cloud Model (Attema & Ulaby, 1978), but the equation was chosen because it had a higher $r^2$ than any other relationship that was tested, rather than for theoretical reasons. For this analysis, data points were weighted according to the square root of their area (Zar, 2007), to correct for the differences between the sizes of the sample plots. The fitted relationship was:

$$ALOS\ HV_{sigma^0} = a + b\left[1 - e^{-c.AGB}\right] \quad (5)$$

where $a=-16.59\pm0.46$, $b=4.63\pm0.44$, and $c=0.014\pm0.004$ (uncertainties in parameter estimation are standard errors). The $r^2$ for the fitted regression was 0.86, an F-test for the regression found it to be highly significant ($F_{2,22}=63.23$, $p<0.0001$), and the data passed a Shapiro–Wilk normality test ($p=0.47$).

**Table 1**
Biomass (Mg ha$^{-1}$), stem density (stems ha$^{-1}$), average height (m), basal area (m$^2$ ha$^{-1}$) and ALOS 2007 HH and HV sigma$^0$ (dB) are given for all the field plots. The plot in italics was not used in the biomass regression analysis because it was on a steep slope facing away from the sensor, and thus in radar shadow, whereas the other plots were all from relatively flat ground.

| Biomass Mg ha$^{-1}$ | Stem density stems ha$^{-1}$ | Average height m | Average DBH cm | Basal area m$^2$ ha$^{-1}$ | ALOS HH sigma$^0$ dB | ALOS HV sigma$^0$ dB |
|---|---|---|---|---|---|---|
| 6.1 | 42 | 6.6 | 11.7 | 1.4 | −9.42 | −15.72 |
| 17.4 | 136 | 6.5 | 17.7 | 4.3 | −10.26 | −16.37 |
| 24.9 | 213 | 6.2 | 16.4 | 5.9 | −9.35 | −15.54 |
| 26.3 | 108 | 8.1 | 20.3 | 4.5 | −9.01 | −14.69 |
| 26.4 | 201 | 5.7 | 12.3 | 6.7 | −10.33 | −15.19 |
| 34.5 | 241 | 8.0 | 18.5 | 8.1 | −7.93 | −14.28 |
| 38.4 | 315 | 6.9 | 18.1 | 14.0 | −7.58 | −13.8 |
| 43.2 | 278 | 6.2 | 11.6 | 10.7 | −8.27 | −14.22 |
| 46.3 | 455 | 5.3 | 11.4 | 11.1 | −7.98 | −14.77 |
| 51.4 | 249 | 6.3 | 15.2 | 9.3 | −9.28 | −15.6 |
| 75.1 | 390 | 6.7 | 15.5 | 15.4 | −7.92 | −13.78 |
| 87.2 | 281 | 7.3 | 17.7 | 17.3 | −7.1 | −14.15 |
| 102.9 | 575 | 12.8 | 11.9 | 13.9 | −7.48 | −12.59 |
| 103.1 | 277 | 8.9 | 14.5 | 15.1 | −6.86 | −12.34 |
| 107.8 | 460 | 15.4 | 19.1 | 16.2 | −7.16 | −12.35 |
| 114.7 | 797 | 9.1 | 11.9 | 24.1 | −7.67 | −12.73 |
| 119.7 | 510 | 11.8 | 14.7 | 18.7 | −7.02 | −13.2 |
| 141.2 | 473 | 12.0 | 12.4 | 22.6 | −7.29 | −12.65 |
| 204.4 | 642 | 13.6 | 13.9 | 27.7 | −6.45 | −11.99 |
| 212.3 | 465 | 13.6 | 20.3 | 25.6 | −7.34 | −12.26 |
| 240.5 | 467 | 16.8 | 20.8 | 25.6 | −7.94 | −11.98 |
| 247.1 | 641 | 12.5 | 13.4 | 29.7 | −7.34 | −12.33 |
| *306.97* | *611* | *17.4* | *23.1* | *35.6* | *−8.36* | *−13.22* |
| 456.13 | 516 | 14.6 | 24.6 | 50.5 | −6.25 | −12.02 |

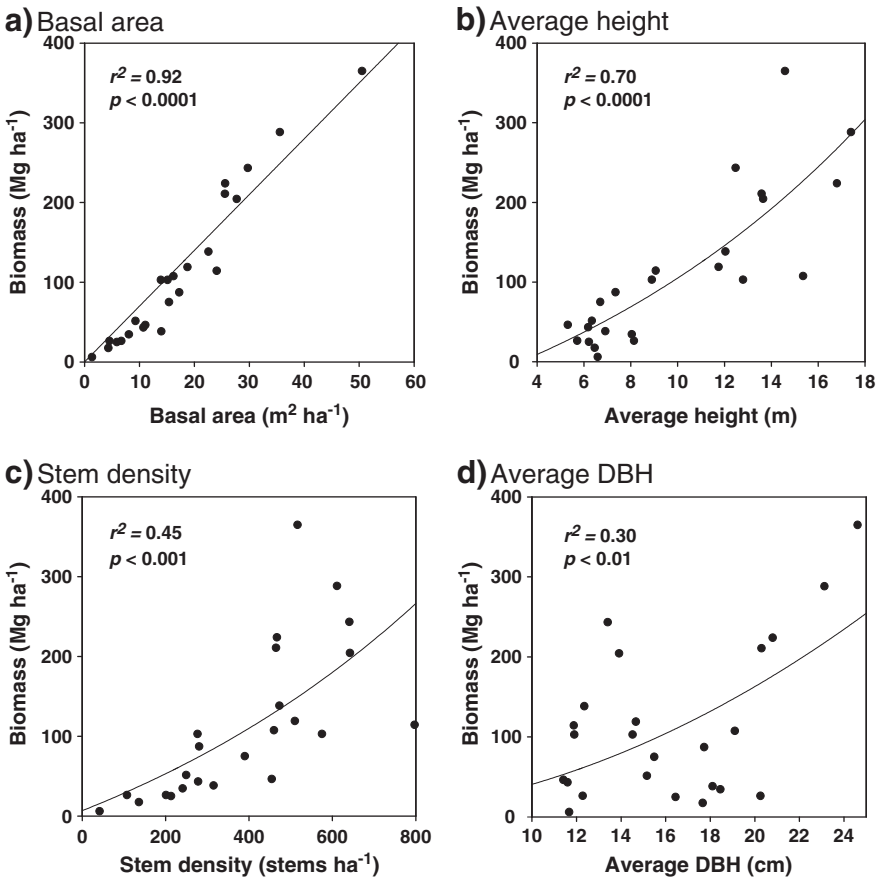


**Fig. 2.** Biomass values for the field plots against a) basal area, b), average height, c) stem density, and d) average DBH. The fit for a is linear, for b, c and d quadratic.

To create a biomass map from the ALOS HV backscatter data Eq. (5) was rearranged to:

$$AGB = \frac{1}{c} \times - \ln\left[1 - \frac{ALOSHV_{sigma^0} - a}{b}\right]. \quad (6)$$

There was also a good, but weaker, relationship with the ALOS HH polarization alone, which gives an estimate of the accuracy of the relationship between JERS HH data from 1996 and AGB ($r^2 = 0.64$, $F_{2,22} = 17.96$, $p < 0.0001$, Fig. 4b).

### 4.4. Accuracy of ALOS-biomass regression

The accuracy of the ALOS HV AGB predictions decrease as biomass increases (Fig. 5). The overall root mean square error (RMSE) for these data is 49 Mg ha$^{-1}$; however this decreases to 29 Mg ha$^{-1}$ if only values below 150 Mg ha$^{-1}$ are considered, and to 24 Mg ha$^{-1}$ using only data points <100 Mg ha$^{-1}$. These results led us to map AGB in classes chosen to be similar in size to the RMSE at each level: 0–25, 25–50, 50–75, 75–100, 100–150, 150–200, and >200 Mg ha$^{-1}$. The large degree of scatter and possible bias observable in Fig. 5 for values >200 Mg ha$^{-1}$ suggests that no subdivision of biomass classes above this point is appropriate.

The relationship between ALOS HH and biomass is clearly noisier, with a loss of sensitivity occurring earlier than for the HV data, at around 100–150 Mg ha$^{-1}$ (Fig. 4b). The RMSE values are consequently higher: 65 Mg ha$^{-1}$ for the whole dataset, 52 Mg ha$^{-1}$ for points <150 Mg ha$^{-1}$, and 39 Mg ha$^{-1}$ for values <100 Mg ha$^{-1}$. Note that the acquisition of these ALOS data was in the wet season, where the HH polarization would be expected to be responding to soil moisture as well as to biomass, and this perhaps explains the poorer than expected performance at lower biomass values. The JERS HH data were captured in the dry season and would therefore be expected to considerably outperform the ALOS HH backscatter. However, to be conservative, it was assumed that the dry season JERS HH is only as accurate as the wet season ALOS HH. Thus much broader biomass classes were used for the JERS data (and thus also the change detection): 0–50, 50–100, 100–150, and >150.

### 4.5. JERS to ALOS-derived biomass regression

A strong relationship was found between the 40 suspected unchanged areas in the JERS HH sigma$^0$ data from March 1996 (dry season) with the ALOS HV biomass data ($r^2 = 0.95$, $F_{2,48} = 341.1$, $p < 0.0001$; Fig. 6). The equation used was identical to Eq. (5), but with coefficients: a = −10.98 ± *0.12*, b = 4.03 ± *0.16*, and c = 0.014 ± *0.002*. The relationship with the JERS HH sigma$^0$ data from November 1996 (wet season) was less strong ($r^2 = 0.72$, data not shown), confirming that radar data are more sensitive to biomass in the dry season. The reason the $r^2$ is higher here than with the ALOS HV data is because of the large areas used to calibrate the relationship (25 ha each), greatly reducing the geolocation errors and noise apparent when a relationship is derived from comparatively small field plots, as in the ALOS to biomass regression. This higher $r^2$ value should not be taken to show that JERS HH is more sensitive to biomass than ALOS HV, as in general its accuracy is likely to be similar to that for ALOS HH (though in all likelihood better as the drier conditions should result in less soil moisture influence). The relationship was used to estimate AGB from JERS HH imagery and a map was produced by classifying AGB into 4 classes with 50 Mg ha$^{-1}$ intervals, chosen to capture the estimation uncertainties predicted using the ALOS HH data (Fig. 7a), the training data is put in the correct class with a 94% accuracy using these classes.

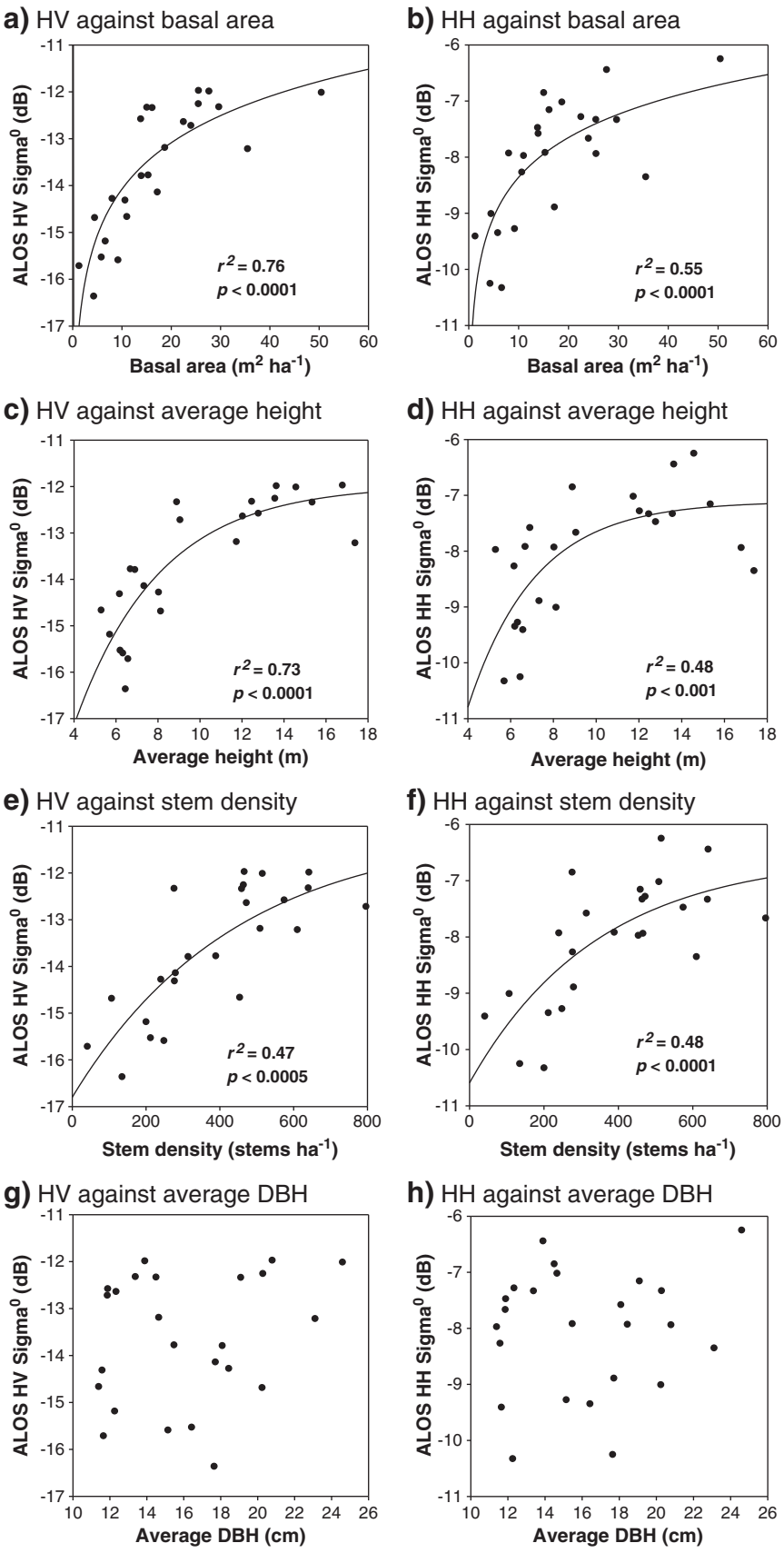


**Fig. 3.** ALOS 2007 HV and HH sigma$^0$ plotted against basal area, average height, stem density and average DBH (stem diameter at 1.3 m). Best fit log relationships were fitted for a–f; no significant relationships were found for g and h.

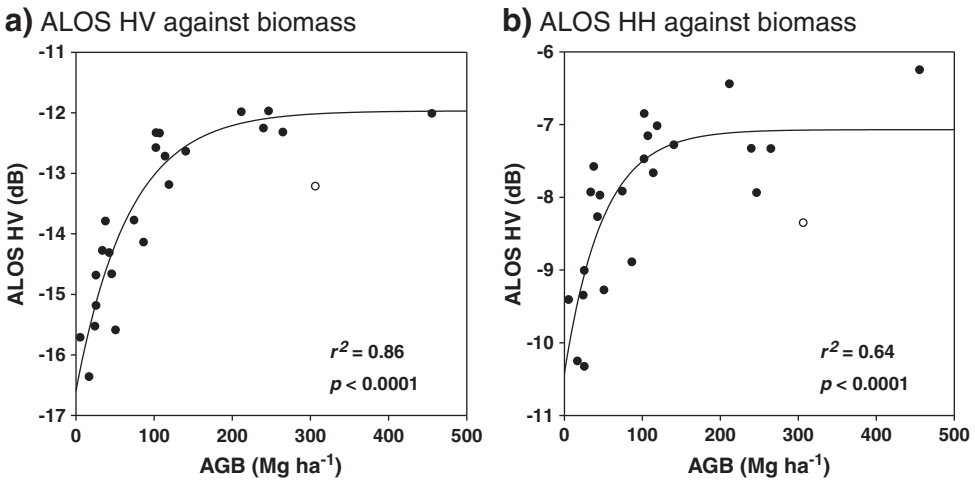


**Fig. 4.** a) ALOS HV sigma$^0$ (dB) and b) ALOS HH sigma$^0$ (dB) plotted against field-measured AGB (Mg ha$^{-1}$), with area-weighted negative exponential relationships fitted. The point in white is from a steep slope and for this reason was excluded from the regression calculations.

For comparison the ALOS HV map with its seven classes is included as Fig. 7b.

### 4.6. Change detection

The biomass change map was produced by tracing the number of biomass classes each 500 m pixel changed between the two periods (Fig. 7c). Although the ALOS biomass map has smaller intervals and a larger biomass range, we produced the change map by using 50 Mg ha$^{-1}$ as the class interval and 150 Mg ha$^{-1}$ as the upper limit, as these are the best that can be confidently predicted using the JERS data. The resulting map shows biomass losses and gains dominating in different parts of the study area, with losses of higher biomass classes in the eastern side, and gains on the western side. Changes in the absolute area covered by each biomass class are also shown in Fig. 8, both for the whole study area, and for the eastern and western sides individually. A loss of the high biomass classes dominates the east of the study area, which appears to be concentrated around the major population centers and along the railway line (Fig. 9). Here the area covered by forest >150 Mg ha$^{-1}$ has declined almost by half, from 2700 km$^2$ in 1996 to 1400 km$^2$ in 2007. However, there are also areas of positive change (i.e. biomass gain), concentrated in the western side of the study area, particularly in the savanna areas of the Mbam Djerem National Park and the area north of it. Increases in biomass appear to occur in all the woodland–savanna areas without a high human population density. These increases are shown by a reduction in the area of biomass classes <100 Mg ha$^{-1}$, and an increase in area for both cover classes >100 Mg ha$^{-1}$.

### 4.7. Uncertainty analysis

There are two major sources of uncertainty in this analysis: uncertainties in calculating biomass values from field data using allometric equations, and uncertainties in using radar remote sensing data to estimate biomass. Uncertainties in the first case seem unlikely to affect the results of the change detection, so increases and decreases should be correctly located, but the magnitude of the biomass classes could be incorrect. Uncertainties inherent in using radar remote sensing data to estimate biomass across an area may, however, affect the results of the change detection, and these errors are particularly uncertain for the JERS data from 1996 as there are no field data, making an assessment of the accuracy of that classification

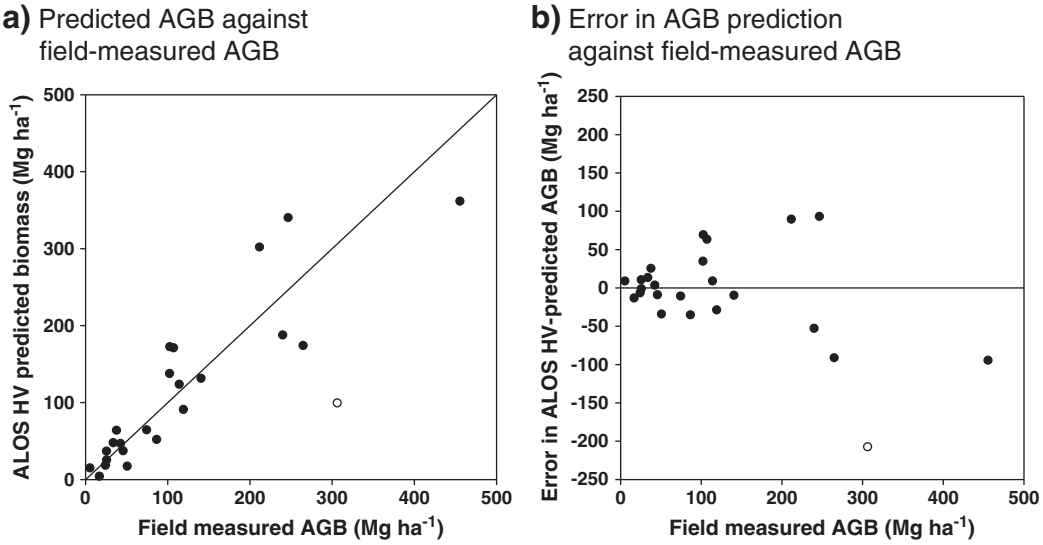


**Fig. 5.** Errors in predicting biomass from the ALOS HV relationship are shown by a) ALOS HV-predicted AGB plotted against field-measured AGB (Mg ha$^{-1}$), with an x = y line shown, and b) the error in ALOS HV biomass prediction plotted against field-measured biomass.

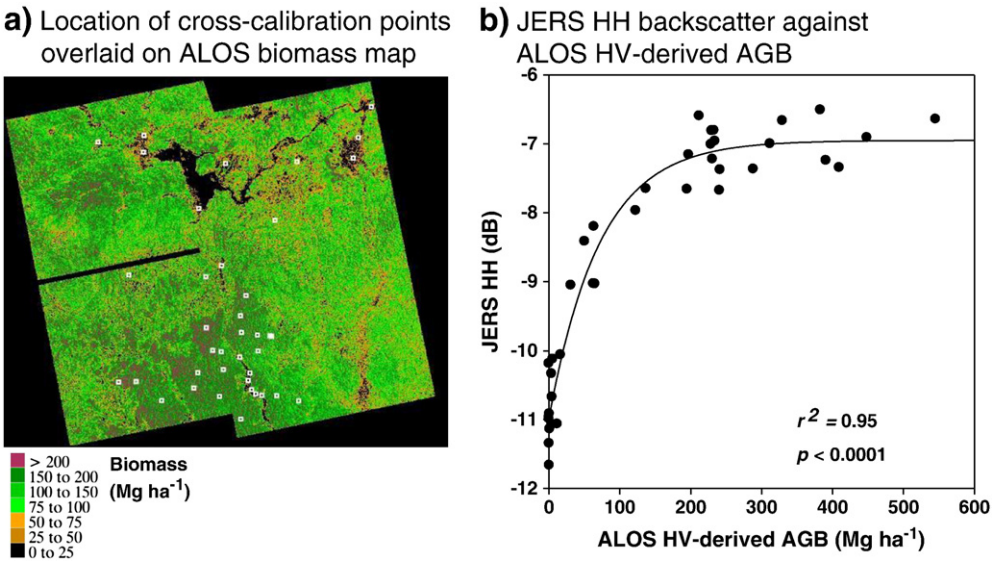


**Fig. 6.** a) Location of 40 × 500 m × 500 m suspected unchanged areas used to back-calibrate JERS HH data to ALOS HV-derived AGB, and b) JERS HH sigma$^0$ from 1996 (dB) plotted against ALOS HV-derived AGB (Mg ha$^{-1}$) from 2007 for these 40 suspected unchanged 25 ha areas.

difficult. Here we will subdivide these uncertainties into their major sources, and estimate the likely contribution from each.

### 4.7.1. Errors in field data to AGB estimation

*4.7.1.1. Uncertainties in diameter, height and species measurements.* Diameter measurements are considered very accurate (Alder & Synnott, 1992), and though height measurements are less precise, an in-field assessment, involving re-measuring 10 trees across the full height range at least 8 times from different angles and on different days, suggested that our methods were accurate to greater than ±10%. All species were identified in the field by expert local botanists, and as such mis-identifications are likely to be relatively few, and given the similarities of wood density within a genus, unlikely to have a major effect on the biomass estimation (Chave et al., 2006, 2009).

*4.7.1.2. Uncertainties in the allometric equation.* It is not possible to use species-specific, or even region-specific, allometric equations for most tropical ecosystems, as the species diversity is too large and the relevant data have not been collected. However using a pan-tropical equation including height, diameter and species-specific wood density minimizes overall uncertainty in biomass estimates to an estimated ±10% (though Chave et al. (2005) optimistically estimate ±5% for the equation we used). This error could be considerably higher for larger trees, where accurate biomass data are very scarce.

We therefore estimate that the biomass classes used could be inaccurate by at worst ±20%, assuming a consistent 10% error in height estimation combined with the allometric equation used that poorly predicts tree biomass and consistently over- or under-estimating by a further 10%. The consequence of this is that, for example, the 100–150 Mg ha$^{-1}$ biomass class could in fact at worst be 80–120 Mg ha$^{-1}$ or 120–180 Mg ha$^{-1}$.

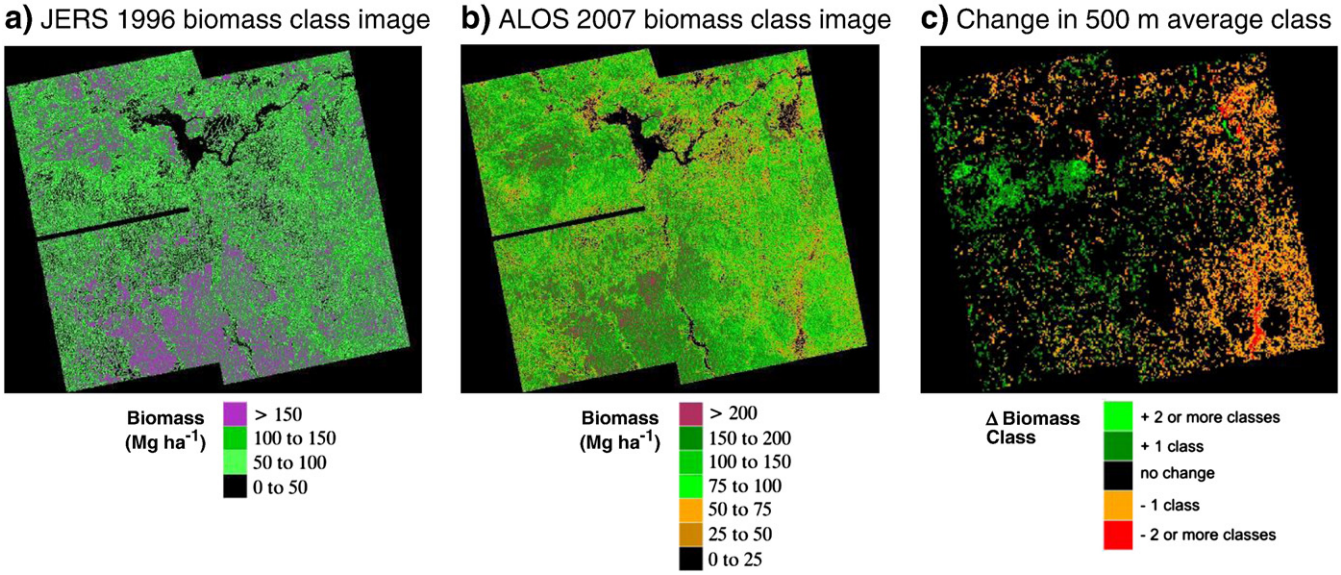


**Fig. 7.** Biomass class images produced using a) JERS HH 1996 data and b) ALOS HV 2007 data, using scales with the size of biomass classes based on RMSE error values, with broader classes for the JERS HH 1996 data than the ALOS HV 2007 data; and c) change in 500 m average class (JERS class image subtracted from ALOS class image) for the two images (using the broader JERS classes).

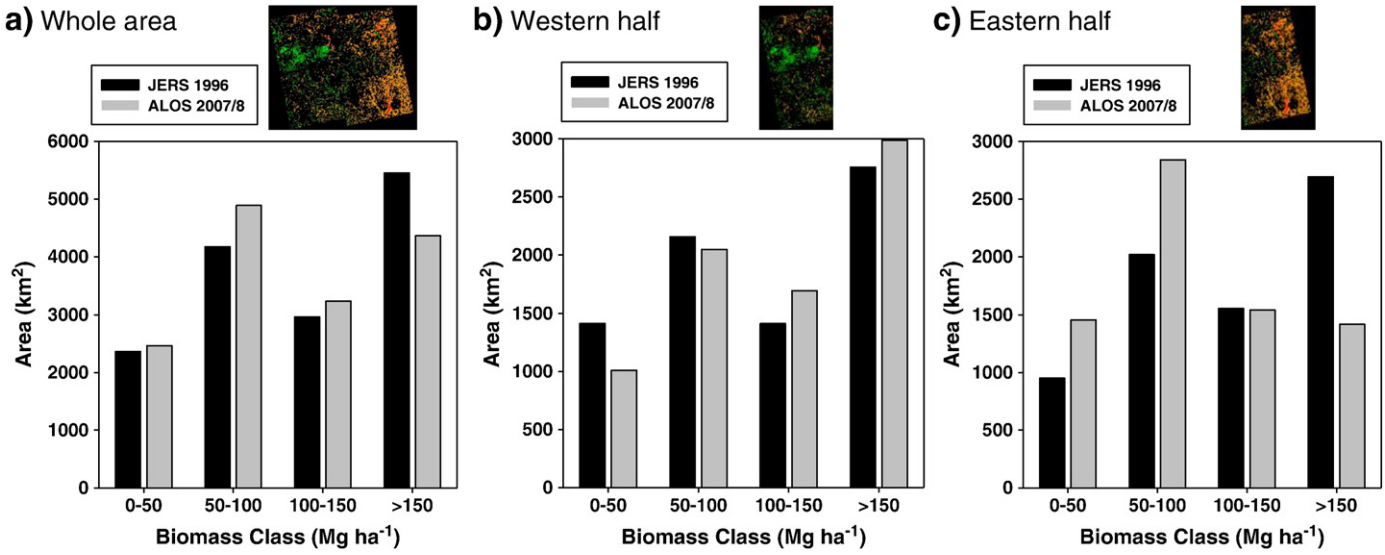


**Fig. 8.** The total area in km$^2$ against biomass class (Mg ha$^{-1}$) for the two biomass maps from 1996 and 2007 for: a) the whole data set; b) the less-populated western half of the study region; and c) the more-populated right hand half.

*4.7.2. Uncertainties in radar to biomass estimation*

We now consider the errors involved in putting a pixel into the correct biomass class. This was estimated using the RMSE values from the original biomass estimation, as discussed in Section 4.5, though these RMSE values are likely to overestimate the true error value because of their small plot size. The biomass class sizes were chosen to be approximately equal to the RMSE values at the respective biomass level. Assuming errors are normally distributed, this should result in approximately 68% of data points being placed in the correct class, and approximately 95% in the correct class or a neighboring class (Zar, 2007). These are indeed approximated in the field data, with 65% of the data points being correctly classified for the ALOS HV data, and 96% being placed in the correct or neighboring class; for ALOS HH (with the wider biomass classes) these values are 57% and 96% respectively.

These errors in classifying pixels should, unlike those for the biomass estimation, be randomly distributed, with no bias (i.e. there is assumed to be an equal chance of over- and under-estimation for every point). Thus while the chances of a randomly chosen pixel being correctly classified is just 66%, the large number of pixels considered in all the classes suggests the overall accuracy in estimating the total area of this class is much higher. This assumption would not be valid if the number of pixels varied

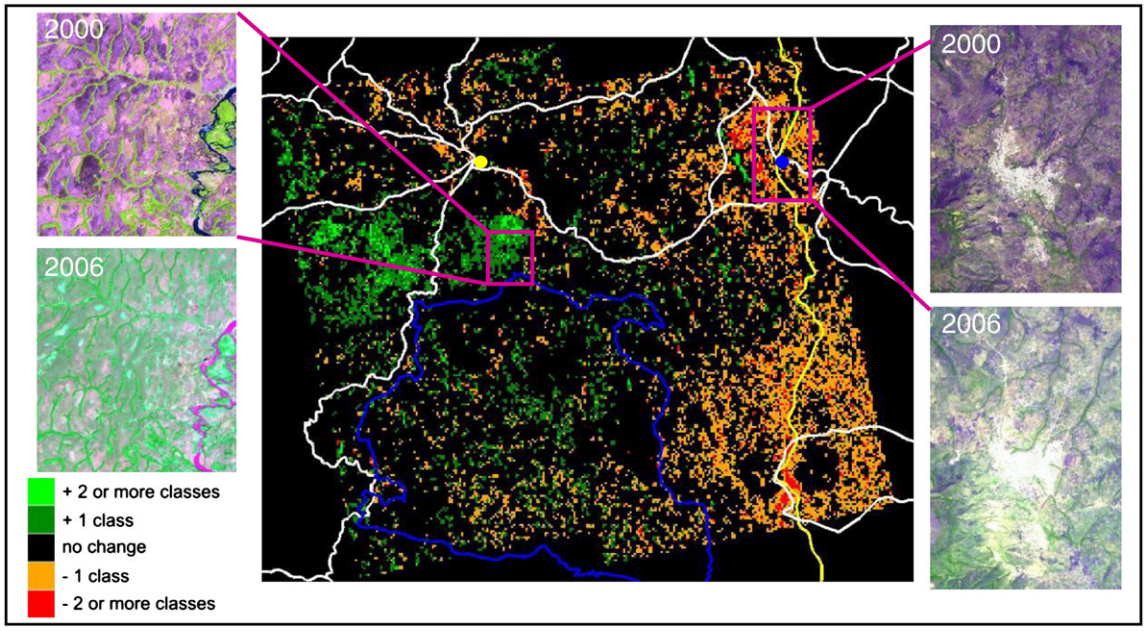


**Fig. 9.** Change in class image using the same method as for Fig. 6c. The major towns of Tibati and Ngaundal are shown as yellow and blue circles respectively, Mbam Djerem National Park is outlined in blue, roads are shown in white, and the railway line in yellow. Optical close-up images are Landsat ETM+ from 2000 (bands 5–4–3) and ASTER from 2006 (bands 3n–2–1), showing the widening of gallery forests and increased woody vegetation on the left-hand pair, and the rapid clearing of woody vegetation around the town of Ngaundal on the right-hand pair. Note that the differences in color are caused by the different bands available from two sensors, however in both the green channel is an infra-red band that responds strongly to vegetation cover, which will mostly be woody in these dry season images.

considerably between classes, as rare classes would be overestimated due to mis-estimation from neighboring classes; however as all the classes are of a similar magnitude this is unlikely to be a serious problem. Equally, 25 pixels are averaged to produce each average class at a 500 m resolution before the change detection routine is performed. Therefore the total area covered by each class in Fig. 8, and the changes in average biomass class at a 500 m resolution in Fig. 7, are thought accurate to at least a 95% (based on a simple statistical simulation model), and possibly higher, suggesting that the changes observed are robust. However, using this methodology to track changes in individual 100 m pixels is likely to give poor estimates, so we produced a biomass change map at a 500 m resolution, as the averaging of the class of 25 pixels gives a level of confidence in the results (>95%) which could not be achieved with a higher resolution (Fig. 7c).

## 5. Discussion

### 5.1. Using radar data to detect changes in forest–savanna ecotones

We detected forest expansion over a large, less-populated western part of our study area, and rapid forest loss in the eastern side. This strongly suggests that satellite L-band SAR data can be used to detect biomass changes in forest–savanna transition regions. While a reduction in signal sensitivity at higher biomasses makes the accurate estimation of forest biomass difficult, detecting changes in the woodiness of savannas, and detecting deforestation and degradation, is possible using a combination of JERS and ALOS PALSAR, and in future with two PALSAR images. The errors in the analysis have been assessed, and shown to be small compared to the signal in the data, increasing our confidence in results derived from L-band SAR data combined with on-the-ground field measurements.

The lack of field data corresponding to the 1996 satellite data increases the error in the results, but apparently not dramatically so; although this error is impossible to quantify precisely, we can be confident in the results given the conservative methodology and broad biomass classes used. These broad classes mean that only pixels that have undergone rapid biomass change will be detected, thus providing confidence that any observed changes are genuine and not caused by noise or mis-calibration of the datasets.

The ALOS data were captured in the wet season, and the HH signal is therefore likely to be less sensitive to differences in biomass than if the imagery had been obtained during the dry season with lower soil moisture influences. Consequently, the HH data from JERS captured in the dry season is likely to have considerably smaller errors than suggested by the ALOS HH data. The benefits of using HV over HH can be seen clearly, with a relationship found with $r^2 = 0.86$ for the ALOS HV data, despite the wet season image capture. This is due to the minimal impact of soil moisture on L-band HV, which has been shown elsewhere (Dubois et al., 1995; Oh et al., 1992).

### 5.2. Forest expansion

The smaller-scale (40–300 $km^2$) reports of Boulvert (1990), Happi (1998) and Guillet et al. (2001) showing woody expansion in Cameroon are consistent with our larger scale (15 000 $km^2$) study: woody expansion is indeed occurring in some forest–savanna transition regions, and it is occurring rapidly, with many pixels increasing by two biomass classes over the eleven year study period, equivalent to at least a doubling in biomass. While this increase is rapid, it is not necessarily unrealistic: increases of 1.4–2.0 Mg $ha^{-1} yr^{-1}$ have been observed in the drier Miombo woodlands (Chidumayo, 1997; Williams et al., 2008), and increases >10 Mg $ha^{-1} yr^{-1}$ have been found for secondary forest growth in Amazonia (Feldpausch et al., 2004; Gehring et al., 2005; Houghton et al., 2000), in wetter, less seasonal conditions. We therefore estimate that increases in the order of 5 Mg $ha^{-1} yr^{-1}$ would be possible in this area, which is sufficient to produce the observed increases over the eleven years.

This also corroborates a recent study using high resolution spectral vegetation index data over a 5000 $km^2$ region equivalent to the central-west section of this study area from 1986 to 2006, which found significant increases in the woody cover of the savanna regions (Mitchard et al., 2009). Equally, this finding agrees with informal independent field observations in the Mbam Djerem National Park: the first 30 m or so of most gallery forests were dominated by young pioneer trees, with a scattering of older dead and dying savanna trees being shaded by the arrival of faster growing and ultimately taller forest biome species (Mitchard et al., 2009 & personal observation by ETAM, TRF, SLL & BS).

It is likely that the expansion of forest is caused by a reduction in human disturbance, especially fire, which may have resulted from a combination of urban migration, changes in lifestyle away from cattle herding, and the formation of the Mbam Djerem National Park. These factors have previously been shown to be the cause of woody encroachment in a number of semi-arid environments in Africa (Dalle et al., 2006; Ward, 2005). Although it is difficult to quantify the total positive effect of the designation of the area as a National Park on biomass gain, the study does show the potential for national parks in forest–savanna ecotone regions to be managed to sequester carbon. It is possible that adopting a policy of limiting savanna burning and exploitation might enable such parks to earn valuable funds, either in the voluntary carbon market or the proposed Reduced Emissions from Deforestation and Degradation (REDD) scheme. By contrast, it demonstrates that a policy of savanna burning may need to be implemented in Mbam Djerem National Park in order to maintain the unique diversity of ecosystem types present.

This study also demonstrates that a combination of satellite radar data with field studies can provide sufficiently robust evidence to claim and validate carbon stocks (though robust baseline data will also be needed to enable calculations of carbon credits). Ideally however a still-more robust analysis would be performed, using L- or P-band data from the same sensor in the same season under similar ground moisture conditions, in combination with field data collected in the same year as each radar scene. This would increase the accuracy and confidence in the results, removing any need for back calibration, and allowing direct estimation of biomass changes per pixel, without the need for broad biomass classes. It would also reduce the influence of soil moisture. The impact of soil moisture in this study cannot be ruled out entirely, although we believe it could not explain the biomass increases observed in this study, because (a) forest–savanna boundaries and gallery forests in the ALOS HV image are clearly visible, (b) these boundaries correspond well with the Quickbird data, and (c) we used a large number of biomass plots and calibration points around the area which showed the biggest biomass increase.

### 5.3. Forest loss

Despite the significant gains shown in the west, the overall biomass trend for the study area is negative, with a net loss of 20% (1090 $km^2$) of high biomass forest (>150 Mg $ha^{-1}$) over the 11 year study period. The losses along the railway line and paved road on the eastern side of the study area are very obvious, and similarly around the town of Ngaoundal in the north-east (Fig. 9). We suspect strongly that this change is due to human-driven deforestation and degradation (SLL personal observation), but cannot rule out the possibility that it is due to forest die-back following a localized drought (Dai et al., 2004). The population density there is higher, and as well as farming and timber extraction for fuel (both woodfuel for local use and charcoal for transport to towns and cities), there are logging operations in the forest areas outside the park. Clearly, the fate of woody vegetation in this region is currently largely in the hands of humans, and without intervention it seems likely that rapid net forest biomass losses will

continue; biomass gains in protected areas are very unlikely to be large enough to offset losses of forest and biomass elsewhere. However, recent population trends leave some room for cautious optimism regarding biomass stocks: although the urban population of Cameroon grew by 3.61% per year from 2002 till 2006, the rural population actually fell slightly, at an average rate of −0.023% per year (World Bank, 2007). Yet, the growing urban population will, of course, have larger demands for fuel, food and timber, so while remote or protected areas may have the potential for an increase in biomass, areas of forest and woody savanna near settlements and access routes are likely to continue to decrease in biomass unless affordable alternatives are available to local biomass-based products. The Mbam Djerem National Park is relatively well protected and the savannas are not currently systematically burned, and as such the land in the park may continue sequestering carbon into the future. Given the rate of loss outside the park, perhaps community projects in this area attempting to reduce deforestation and promote the planting of trees may be more successful at carbon sequestration than relying on natural regeneration within undisturbed savannas (Williams et al., 2008). However, as Geist and Lambin (2002) showed in a meta-analysis of 152 sub-regional deforestation studies, the principal cause of deforestation is demand from remote foreign markets, so local intervention may not alone provide a solution. In addition to local action large-scale, concerted international solutions such as REDD, involving making performance-based payments to reduce deforestation and degradation rates alongside demand management for wood products, may be necessary.

### 5.4. Implications for future radar satellites

While the methods used in this study are sufficient to accurately find areas of large-magnitude biomass change, using these data we cannot be very exact in assessing the precise magnitude of such changes, nor of absolute carbon stocks. However, in the future it is likely to be possible to produce quantitative estimates of biomass change using radar backscatter images captured during the same season over different years from identical or similar L- or P-band polarimetric sensors. The similar geometric configuration and radiometric accuracy of the sensors will allow the use of established radar change detection algorithms which directly compare backscatter values (Carincotte et al., 2006; Rignot & Vanzyl, 1993; Touzi et al., 1999). This will be possible using ALOS PALSAR data (which will be continued by ALOS-2), but also with more informative data including information about tree heights from new satellites such as NASA's interferometric L-band SAR and lidar DESDynI, and ESA's planned interferometric P-band BIOMASS. Such data should allow for accurate large-scale, high resolution and long-term monitoring of forest degradation and regeneration.

It is also possible that the accuracy of the biomass maps produced at each time point could be improved by the addition of optical data and digital elevation models (DEMs) to the radar data, using multivariate analysis techniques. Optical data, such as vegetation indices, provide a different suite of information about forest structure in these ecosystems (for example canopy cover; Mitchard et al., 2009) that might be beneficial in producing more robust biomass maps, and DEMs could be used to correct for the influence of slope on radar backscatter. This technique of incorporating many different layers to produce biomass maps has been conducted at a coarse resolution in Amazonia (e.g. Saatchi et al., 2007), but would suffer from the difficulties of acquiring comparable, high resolution and cloud-free images captured at a similar time to the radar images for each year for this kind of high resolution change detection. In general, however, more information should provide greater constraints on potential errors and improve accuracy, so this type of combined-data approach should be investigated.

## Acknowledgments

The authors would like to acknowledge Gatsby Plants for providing ETAM's PhD studentship, and TROBIT, a NERC-funded consortium, grant ref: NE/D005590/1, for funding the rest of the work. SLL was funded by a Royal Society University Research Fellowship. Jon Lloyd, TROBIT P.I., provided useful advice and expertise. Three anonymous referees provided helpful suggestions and comments on an earlier version of the manuscript that were instrumental in improving the study. Adam Freedman provided advice on the sources of accurate population data. Jeanette Sonké, Wildlife Conservation Society-Cameroon (WCS-Cameroon), The University of Yaounde I, and 14 canoeists from Mbakaou provided invaluable support in Cameroon. Remote sensing data were provided by the Alaska Satellite Facility, the Global Rainforest Mapping Project, NASA and Eurimage; Landsat and ASTER images were provided free of charge by Terralook, courtesy of USGS EROS and NASA's Jet Propulsion Laboratory; TRMM 3B43 data was downloaded from the Giovanni online data system, developed and maintained by the NASA Goddard Earth Sciences (GES) Data and Information Services Center (DISC).

## References

Alder, D., & Synnott, T. J. (1992). Permanent sample plot techniques for mixed tropical forest. *Oxford Forestry Institute Tropical Forestry Papers*, *25*.

Anonymous (2007). *Park National du Mbam et Djerem, Plan d'Aménagement 2007–2011*. Cameroun: Le Ministère des Forêts et de la Faune.

Archer, S., Boutton, T. W., & Hibbard, K. A. (2001). Trees in grasslands: Biogeochemical consequences of woody plant expansion. In E. -D. Schulze, S. Harrison, M. Heimann, E. Holland, J. Lloyd, I. Prentice, & D. Schimel (Eds.), *Global biogeochemical cycles in the climate system* (pp. 115–133). San Diego: Academic Press.

Attema, E. P. W., & Ulaby, F. T. (1978). Vegetation modeled as a water cloud. *Radio Science*, *13*, 357–364.

Boulvert, Y. (1990). Avancée ou recul de la forêt centroafricaine. Changements climatiques, influence de l'homme et notamment de feux. In R. Lanfranchi, & D. Schwartz (Eds.), *Paysages Quaternaries de l'Afrique Central Atlantique* (pp. 353–366). Paris: Initiations et Didactiques ORSTROM.

Bowman, D., Walsh, A., & Milne, D. J. (2001). Forest expansion and grassland contraction within a Eucalyptus savanna matrix between 1941 and 1994 at Litchfield National Park in the Australian monsoon tropics. *Global Ecology and Biogeography*, *10*, 535–548.

Brook, B. W., & Bowman, D. (2006). Postcards from the past: Charting the landscape-scale conversion of tropical Australian savanna to closed forest during the 20th century. *Landscape Ecology*, *21*, 1253–1266.

Bucini, G., & Hanan, N. P. (2007). A continental-scale analysis of tree cover in African savannas. *Global Ecology and Biogeography*, *16*, 593–605.

Carincotte, C., Derrode, S., & Bourennane, S. (2006). Unsupervised change detection on SAR images using fuzzy hidden Markov chains. *IEEE Transactions on Geoscience and Remote Sensing*, *44*, 432–441.

Center for International Earth Science Information Network (CIESIN) Columbia University, International Food Policy Research Institute (IPFRI), World Bank, & Centro Internacional de Agricultura Tropical (CIAT) (2004). *Global Rural–Urban Mapping Project (GRUMP): Urban/Rural Population grids*. Palisades, NY: CIESIN, Columbia University Downloaded from http://sedac.ciesin.columbia.edu/gpw/.

Chave, J., Andalo, C., Brown, S., Cairns, M. A., Chambers, J. Q., Eamus, D., et al. (2005). Tree allometry and improved estimation of carbon stocks and balance in tropical forests. *Oecologia*, *145*, 87–99.

Chave, J., Coomes, D., Jansen, S., Lewis, S. L., Gwenson, N. G., & Zanne, A. E. (2009). Towards a worldwide wood economics spectrum. *Ecology Letters*, *12*, 351–366.

Chave, J., Muller-Landau, H. C., Baker, T. R., Easdale, T. A., Ter Steege, H., & Webb, C. O. (2006). Regional and phylogenetic variation of wood density across 2456 neotropical tree species. *Ecological Applications*, *16*, 2356–2367.

Chidumayo, E. N. (1997). *Miombo ecology and management: An introduction*. London: IT Publications in association with the Stockholm Environment Institute.

Dai, A. G., Trenberth, K. E., & Qian, T. T. (2004). A global dataset of Palmer Drought Severity Index for 1870–2002: Relationship with soil moisture and effects of surface warming. *Journal of Hydrometeorology*, *5*, 1117–1130.

Dalle, G., Maass, B. L., & Isselstein, J. (2006). Encroachment of woody plants and its impact on pastoral livestock production in the Borana lowlands, southern Oromia, Ethiopia. *African Journal of Ecology*, *44*, 237–246.

De Grandi, G., Mayaux, P., Rauste, Y., Rosenqvist, A., Simard, M., & Saatchi, S. S. (2000). The Global Rain Forest Mapping Project JERS-1 radar mosaic of tropical Africa: Development and product characterization aspects. *IEEE Transactions on Geoscience and Remote Sensing*, *38*, 2218–2233.

Doumenge, C., Ndinga, A., Nembot, T. F., Tchanou, Z., Ondo, V. M., Nze, N. O., et al. (2003). Forest biodiversity conservation in Atlantic regions of central Africa: II. Identifying a network of critical sites. *Bois et Forest des Tropiques*, *296*, 43–58.

Duarte, L. D. S., Machado, R. E., Hartz, S. M., & Pillar, V. D. (2006). What saplings can tell us about forest expansion over natural grasslands. *Journal of Vegetation Science*, *17*, 799–808.

Dubois, P. C., Vanzyl, J., & Engman, T. (1995). Measuring soil-moisture with imaging radars. *IEEE Transactions on Geoscience and Remote Sensing*, *33*, 915–926.

Durigan, G., & Ratter, J. A. (2006). Successional changes in cerrado and cerrado/forest ecotonal vegetation in western Sao Paulo State, Brazil, 1962–2000. *Edinburgh Journal of Botany*, *63*, 119–130.

Eamus, D., & Palmer, A. (2007). Is climate change a possible explanation for woody thickening in arid and semi-arid regions? *Research Letters in Ecology*.

FAO (2007). *State of the world's forests 2007*. Rome: Food and Agriculture Organization of the United Nations.

Feldpausch, T. R., Rondon, M. A., Fernandes, E. C. M., Riha, S. J., & Wandelli, E. (2004). Carbon and nutrient accumulation in secondary forests regenerating on pastures in central Amazonia. *Ecological Applications*, *14S*, S164–S176.

Gehring, C., Denich, M., & Vlek, P. L. G. (2005). Resilience of secondary forest regrowth after slash-and-burn agriculture in central Amazonia. *Journal of Tropical Ecology*, *21*, 519–527.

Geist, H. J., & Lambin, E. F. (2002). Proximate causes and underlying driving forces of tropical deforestation. *Bioscience*, *52*, 143–150.

Goetze, D., Horsch, B., & Porembski, S. (2006). Dynamics of forest–savanna mosaics in north-eastern Ivory Coast from 1954 to 2002. *Journal of Biogeography*, *33*, 653–664.

Guillet, B., Achoundong, G., Happi, J. Y., Beyala, V. K. K., Bonvallot, J., Riera, B., et al. (2001). Agreement between floristic and soil organic carbon isotope (C-13/C-12, C-14) indicators of forest invasion of savannas during the last century in Cameroon. *Journal of Tropical Ecology*, *17*, 809–832.

Happi, J. Y. (1998). *Arbres contre graminees: la lenta invasion de la savane par la foret au center-Cameroun.* Paris: Université de Paris Sorbonne.

Hely, C., Bremond, L., Alleaume, S., Smith, B., Sykes, M. T., & Guiot, J. (2006). Sensitivity of African biomes to changes in the precipitation regime. *Global Ecology and Biogeography*, *15*, 258–270.

Hopkins, M. S., Head, J., Ash, J. E., Hewett, R. K., & Graham, A. W. (1996). Evidence of a Holocene and continuing recent expansion of lowland rain forest in humid, tropical North Queensland. *Journal of Biogeography*, *23*, 737–745.

Houghton, R. A., Skole, D. L., Nobre, C. A., Hackler, J. L., Lawrence, K. T., & Chomentowski, W. H. (2000). Annual fluxes of carbon from deforestation and regrowth in the Brazilian Amazon. *Nature*, *403*, 301–304.

Hovestadt, T., Yao, P., & Linsenmair, K. E. (1999). Seed dispersal mechanisms and the vegetation of forest islands in a West African forest–savanna mosaic (Comoe National Park, Ivory Coast). *Plant Ecology*, *144*, 1–25.

Jeltsch, F., Moloney, K., & Milton, S. J. (1999). Detecting process from snapshot pattern: Lessons from tree spacing in the southern Kalahari. *Oikos*, *85*, 451–466.

Lewis, S. L. (2006). Tropical forests and the changing Earth system. *Philosophical Transactions of the Royal Society of London Series B-Biological Sciences*, *361*, 195–210.

Lewis, S. L., Lopez-Gonzalez, G., Sonke, B., Affum-Baffoe, K., Baker, T. R., Ojo, L. O., et al. (2009). Increasing carbon storage in intact African tropical forests. *Nature*, *457*, 1003-U1003.

Lewis, S. L., Malhi, Y., & Phillips, O. L. (2004). Fingerprinting the impacts of global change on tropical forests. *Philosophical Transactions of the Royal Society of London Series B-Biological Sciences*, *359*, 437–462.

Lloyd, J., & Farquhar, G. D. (1996). The $CO_2$ dependence of photosynthesis, plant growth responses to elevated atmospheric $CO_2$ concentrations and their interaction with soil nutrient status. 1. General principles and forest ecosystems. *Functional Ecology*, *10*, 4–32.

Lloyd, J., & Farquhar, G. D. (2008). Effects of rising temperatures and [$CO_2$] on the physiology of tropical forest trees. *Philosophical Transactions of the Royal Society B-Biological Sciences*, *363*, 1811–1817.

Loveland, T. R., Reed, B. C., Brown, J. F., Ohlen, D. O., Zhu, Z., Yang, L., et al. (2000). Development of a global land cover characteristics database and IGBP DISCover from 1 km AVHRR data. *International Journal of Remote Sensing*, *21*, 1303–1330.

Lu, D. S. (2006). The potential and challenge of remote sensing-based biomass estimation. *International Journal of Remote Sensing*, *27*, 1297–1328.

Lucas, R. M., Milne, A. K., Cronin, N., Witte, C., & Denham, R. (2000). The potential of synthetic aperture radar (SAR) for quantifying the biomass of Australia's woodlands. *Rangeland Journal*, *22*, 124–140.

Marimon, B. S., Lima, E. S., Duarte, T. G., Chieregatto, L. C., & Ratter, J. A. (2006). Observations on the vegetation of northeastern Mato Grosso, Brazil. IV. An analysis of the cerrado-Amazonian forest ecotone. *Edinburgh Journal of Botany*, *63*, 323–341.

Mayaux, P., Bartholome, E., Fritz, S., & Belward, A. (2004). A new land-cover map of Africa for the year 2000. *Journal of Biogeography*, *31*, 861–877.

Menaut, J. C. (1983). The vegetation of African savanna. In F. Bourliere (Ed.), *Ecosystems of the world: Tropical savannas*. Amsterdam: Elsevier.

Mertens, B., & Lambin, E. F. (2000). Land-cover-change trajectories in southern Cameroon. *Annals of the Association of American Geographers*, *90*, 467–494.

Mitchard, E. T. A., Saatchi, S. S., Gerard, F. F., Lewis, S. L., & Meir, P. (2009). Measuring woody encroachment along a forest–savanna boundary in central Africa. *Earth Interactions*, *13*, 8.

Nangendo, G. v. S. O. d. G. A. (2005). Biodiversity conservation through burning: a case study of woodlands in Budongo Forest Reserve, NW Uganda. In M. A. F. D. T. Ros-Tonen (Ed.), *African forests between nature and livelihood resources: interdisciplinary studies in conservation and forest management* (pp. 113–128). New York: The Edin Mellen Press.

Oh, Y., Sarabandi, K., & Ulaby, F. T. (1992). An empirical-model and an inversion technique for radar scattering from bare soil surfaces. *IEEE Transactions on Geoscience and Remote Sensing*, *30*, 370–381.

PNUD (UNDP, United Nations Development Program). (1999). *Rapport sur le pauvreté rurale au Cameroun.* Yaoundé: PNUD.

Podest, E., & Saatchi, S. (2002). Application of multiscale texture in classifying JERS-1 radar data over tropical vegetation. *International Journal of Remote Sensing*, *23*, 1487–1506.

Puyravaud, J. P., Dufour, C., & Aravajy, S. (2003). Rain forest expansion mediated by successional processes in vegetation thickets in the Western Ghats of India. *Journal of Biogeography*, *30*, 1067–1080.

Ratter, J. A. (1992). Transitions between cerrado and forest vegetation in Brazil. In P. A. Furley, J. Proctor, & J. A. Ratter (Eds.), *Nature and dynamics of forest–savanna boundaries*. London: Chapman and Hall.

Ribeiro, N. S., Saatchi, S. S., Shugart, H. H., & Washington-Allen, R. A. (2008). Aboveground biomass and Leaf Area Index (LAI) mapping for Niassa Reserve, northern Mozambique. *Journal of Geophysical Research-Biogeosciences*, *113*.

Rignot, E. J. M., & Vanzyl, J. J. (1993). Change detection techniques for Ers-1 Sar Data. *IEEE Transactions on Geoscience and Remote Sensing*, *31*, 896–906.

Rosenqvist, A., Shimada, M., & Milne, A. K. (2007). *The ALOS Kyoto & Carbon Initiative* (pp. 3614–3617)..

Saatchi, S. S., Houghton, R. A., Alvala, R., Soares, J. V., & Yu, Y. (2007). Distribution of aboveground live biomass in the Amazon basin. *Global Change Biology*, *13*, 816–837.

Sankaran, M., Hanan, N. P., Scholes, R. J., Ratnam, J., Augustine, D. J., Cade, B. S., et al. (2005). Determinants of woody cover in African savannas. *Nature*, *438*, 846–849.

Sano, E. E., Ferreira, L. G., & Huete, A. R. (2005). Synthetic aperture radar (L band) and optical vegetation indices for discriminating the Brazilian savanna physiognomies: A comparative analysis. *Earth Interactions*, *9*.

Santos, J. R., Lacruz, M. S. P., Araujo, L. S., & Keil, M. (2002). Savanna and tropical rainforest biomass estimation and spatialization using JERS-1 data. *International Journal of Remote Sensing*, *23*, 1217–1229.

Shimada, M., Isoguchi, O., Tadono, T., & Isono, K. (2009). PALSAR radiometric calibration and geometric calibration. *IEEE Transactions on Geoscience and Remote Sensing*, *47*, 3915–3932.

Smith, T. B., Kark, S., Schneider, J., Wayne, R. K., & Moritz, C. (2001). Biodiversity hotspots and beyond: The need for preserving environmental transitions. *Trends in Ecology and Evolution*, *16*, 431.

Smith, T. B., Wayne, R. K., Girman, D. J., & Bruford, M. W. (1997). A role for ecotones in generating rainforest biodiversity. *Science*, *276*, 1855–1857.

Taiz, L., & Zeiger, E. (2006). *Plant physiology* (4th Edition). Sunderland, MA: Sinauer Associates.

Touzi, R., Lopes, A., Bruniquel, J., & Vachon, P. W. (1999). Coherence estimation for SAR imagery. *IEEE Transactions on Geoscience and Remote Sensing*, *37*, 135–149.

Ward (2005). Do we understand the causes of bush encroachment in African savannas? *African Journal of Range and Forage Science*, 101–105.

Williams, M., Ryan, C. M., Rees, R. M., Sarnbane, E., Femando, J., & Grace, J. (2008). Carbon sequestration and biodiversity of re-growing Miombo woodlands in Mozambique. *Forest Ecology and Management*, *254*, 145–155.

Woodhouse, I. H. (2005). *Introduction to microwave remote sensing.* CRC Press.

Woodhouse, I. H. (2006). Predicting backscatter-biomass and height-biomass trends using a macroecology model. *IEEE Transactions on Geoscience and Remote Sensing*, *44*, 871–877.

World Bank (2007, March). *World Bank Development Indicators Database.* Washington DC: World Bank Accessed online at http://www.worldbank.org/data/onlinedatabases/wdi.

Zanne, A. E., Lopez-Gonzalez, G., Coomes, D. A., Ilic, J., Jansen, S., Lewis, S. L., et al. (2009). *Global wood density database.* Dryad http://hdl.handle.net/10255/dryad.235.

Zar, J. H. (2007). *Biostatistical analysis* (5th Edition). USA: Prentice-Hall.

Zeng, N., & Neelin, J. D. (2000). The role of vegetation–climate interaction and interannual variability in shaping the African savanna. *Journal of Climate*, *13*, 2665–2670.

Zhang, Q. F., Justice, C. O., Jiang, M. X., Brunner, J., & Wilkie, D. S. (2006). A GIS-based assessment on the vulnerability and future extent of the tropical forests of the Congo Basin. *Environmental Monitoring and Assessment*, *114*, 107–121.